The Astrophysical Journal, 836:220 (7pp), 2017 February 20 https://doi.org/10.3847/1538-4357/836/2/220

Blazar Jets Perturbed by Magneto-gravitational Stresses in Supermassive Binaries

A. Cavaliere[1,2], M. Tavani[1,2,3,4], and V. Vittorini[2]
[1] Astronomia, Accademia Nazionale dei Lincei, via della Lungara 10, I-00165 Roma, Italy
[2] INAF/IAPS–Roma, via del Fosso del Cavaliere 100, I-00133 Roma, Italy
[3] Universitá "Tor Vergata", Dipartimento di Fisica, via della Ricerca Scientifica 1, I-00133 Roma, Italy
[4] Gran Sasso Science Institute, viale Francesco Crispi 7, I-67100 L'Aquila, Italy
Received 2016 July 27; revised 2017 January 2; accepted 2017 January 8; published 2017 February 22

Abstract

We study particle acceleration and radiative processes in blazar jets under recurring conditions set by gravitational perturbations in supermassive binary systems. We consider the action from a companion orbiting a primary black hole of $\sim 10^8\,M_\odot$, and perturbing its relativistic jet. We discuss how such conditions induce repetitive magneto-hydrodynamic stresses along the jet, and affect its inner electron acceleration and radiative processes. Specifically, we study how macroscopic perturbations related to increased jet "magnetization" end up in higher radiative outputs in the optical, X-ray, and gamma-ray bands. We first find an increase in magnetic field strength, as gauged in the optical band from the synchrotron emission of electrons accelerated in kinetic processes stimulated by reconnecting magnetic lines. The energetic electrons then proceed to up-scatter the synchrotron photons to GeV energies after the canonical synchrotron self-Compton radiation process. Our model implies a specific recurring pattern in the optical to gamma-ray emissions, made of high peaks and wide troughs. Progressing accelerations caused by spreading reconnections will produce an additional synchrotron keV component. Such outbursts provide a diagnostics for enhanced acceleration of electrons, which can up-scatter photons into the TeV range. We discuss how our model applies to the BL Lac object PG 1553+113, arguably the best candidate to now for high amplitude, recurring modulations in its gamma-ray emissions. We also consider other BL Lacs showing correlated keV–TeV radiations such as Mrk 421.

Key words: BL Lacertae objects: individual (PG 1553+113, Mrk 421) – gamma rays: general – galaxies: active

1. Introduction

Blazars are singled out among the active galactic nuclei (AGNs) by their relativistically collimated jets with bulk Lorentz factors $\Gamma \sim 5$–15 (Urry & Padovani 1995). They are launched by a central supermassive black hole (SMBH) with mass $M\ 10^8\,M_\odot$, and are Doppler-boosted when a jet happens to be closely aligned with our line of sight.

Blazars are extreme in several respects. The observed outputs are very bright, up to $10^{49}\,\mathrm{erg\,s^{-1}}$ in isotropic extrapolation, and strongly variable on diverse timescales from years to minutes, depending on the observed bands. They show highly *non-thermal* spectra with energy distributions (SEDs) constituted by two humps: one peaking in the *IR*–UV bands of clear synchrotron (S) origin; the other extending from hard X- to gamma-rays, of likely inverse Compton (IC) nature (for basics, see Rybicki & Lightman 1979). Both are produced by highly relativistic electrons with random Lorentz factors up to $\gamma_p \sim 10^3$ that inhabit the jets.

Two main blazar flavors are discerned (see Peterson 1997; Ghisellini 2016). The BL Lac-type sources feature two comparable spectral humps, while many flat spectrum radio quasars (FSRQs) feature Compton-dominated spectra at gamma-ray energies, but also a conspicuous big blue bump and the strong, broad optical emission lines common to many quasars. Accelerated particles within the relativistic jet emit by synchrotron (S) radiation an observed (and isotropically extrapolated) luminosity $L_S \propto n\,R^3\,B^2\,\gamma_p^2\,\Gamma^4$, in terms of the density n of relativistic electrons within the source size R, and of the general magnetic field $B \sim 1$ G threading the jet. On the other hand, the IC scattering operates on "seed" photons, conserving their number while upgrading their energy by another factor γ_p^2, so as to yield photon energies $h\,\nu \sim h\,\nu_s\,\gamma_p^2$ and related luminosities $L_C \propto L_s\,R\,n\,\gamma_p^2$.

The simplest source structure envisages as seeds the very S photons that are radiated by a single population of relativistic electrons in one homogeneous zone of the jet, so as to also yield a beamed flux of gamma-rays $L_C \sim L_S\,n\,R\,\gamma_p^2$. Such a synchrotron self-Compton (SSC) radiation process (e.g., Maraschi et al. 1992) is sufficient to account also for the gamma-ray outputs in tight correlation with O–X, as featured by many BL Lacs in their quiescent states.

An interesting development is constituted by growing hints or signs of apparently recurrent emissions in a number of blazars—BL Lacs in particular. In this paper we will focus our attention on the origin and modeling of these phenomena.

2. A Binary Driver of Recurring Jet Instabilities

Interest in binary, massive BHs in AGNs started with Begelman et al. (1980), and it is currently being spurred by the recent detections of bursts of gravitational waves constituting the events GW 150914 (Abbott et al. 2016a) and GW 151226 (Abbott et al. 2016b). These events have been shown to originate from binary systems of BHs with intermediate masses $M \sim 50\,M_\odot$. The pairs have been caught in their late inspiral stages, as they were accelerating their orbital motions under increasing energy loss in gravitational waves to end up in catastrophic coalescence, as predicted. In fact, extensive numerical work concerning binary BHs long predated those events, aimed at including *electromagnetic* outputs from systems composed of two BHs and a warm disk or ring of gas (see Palenzuela et al. 2010, and the review by Baumgarte &

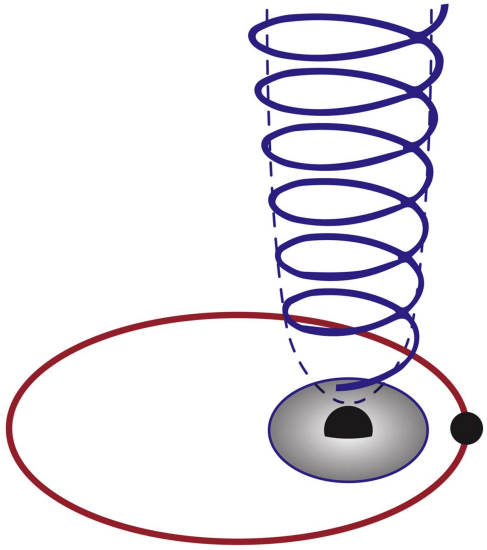

Figure 1. A schematic of our model for the SMBH binary system underlying a BL Lac blazar. The primary SMBH produces a relativistic jet towering well above its formation region in the inner accretion disk (the boundary marked by the thin curve). A SMBH companion orbits around the system barycenter close to the primary, following the red orbit. The gravitational force affects the jet base during its passes close to the periastron, modulating its emissions to a pattern with high peaks followed by long relaxations. The orbital size is of order 10^{16} cm for a total mass around $\sim 10^8\, M_\odot$, mass ratio $M_2/M_1 \sim 10^{-1}$, with an intrinsic period $T \simeq 1.5$ years.

Shapiro 2011). Similar events are also expected in binary systems of two SMBHs (see Colpi 2014; Volonteri et al. 2015).

Ever as such emissions are dramatically enhanced during the final coalescence, they are numerically found to set in gently at much lower rates during the early, long inspiral stage. Similar computations can also be focused on investigating the initially slow evolution of nearly Keplerian orbits and their interactions with the accretion disk; we aim at understanding *nonlinear* light curve shapes recurring on scales of a few years in the EM emissions, as suggested by current gamma-ray observations discussed in Sections 3 and 4.

The emissions of all blazars are governed by the hydrodynamic and magnetic properties of the jet's relativistic plasma outflow (see Section 1). Jet formation and launching in many such sources appear to persist on gross average over timescales of many years. The considerable short term variations observed in their radiative outputs have often been considered to be fully erratic (see, e.g., Kelly et al. 2009). Jet formation and its short term instabilities are then attributed to random variability in the boundary conditions occurring at the base, such as accretion rate; alternatively, disk instabilities (see Nixon & King 2015, and references therein) have been computed and discussed. In the present paper we consider an additional possibility.

We will investigate the binary SMBH scenario depicted in Figure 1, where the primary launches a main jet that dominates the observed fluxes, but is perturbed by the secondary to a considerable degree. We will compute this by considering the binary dynamics of a system with a total mass of $\sim 10^8\, M_\odot$, mass ratio $M_2/M_1 \sim 10^{-1}$, and a current orbital size around several milli-pc. Specifically, the bulk properties of the main jet are affected by episodes of shaking, squeezing, and twisting caused by differential gravitational and electromagnetic stresses along the non-circular, or even not simply Keplerian orbits. The results include time-modulations of the average *strength* $B(t)$ of the magnetic field, coordinated with changes in the local *topology* of B-lines by reconnecting and rearranging those that angularly diverge across narrow layers, as we will discuss in the next section.

Here we just note that passive geometrical effects of gentle beam redirection along steadily curved or helical jets as advocated (e.g., by Raiteri et al. 2015, and Ackermann et al. 2015, henceforth A15) may be reinterpreted in terms of initially mild and slow dynamical effects that take place during the quasi-period. Our discussion will focus instead onto the dynamical *driving* in the jet of sites suitable for magnetic reconnections (MRs) to take place.

3. Unstable Jets

We consider how the progression from large-scale jet instabilities proceeds through an intermediate stage of tearing perturbations to end up in kinetic effects that spread out electron acceleration to high energies.

We base our discussion on the canonical SSC radiation process recalled in Section 1. As with the primary S emission, we adopt standard values of the average magnetic field $B \sim 10^{-1} - 1$ G in the source frame, at the height of some 10^{17} cm above the primary SMBH. These are modulated in time by factors of about three on timescales of a few years by compressing and bending B as discussed later.

The other basic component for S emission is constituted by highly relativistic electrons. Their acceleration occurs in regions within the jet that are affected by magnetic field lines packed, sheared, and reconnected so as to induce macroscopic and kinetic effects. For a review covering the MR theory and the ongoing numerical simulations, see Kagan et al. (2015) and also Melzani et al. (2014). For recent theoretical developments on reconnecting structures in collisionless plasmas, see Coppi (2016); for detailed observational results concerning reconnections in a magnetospheric environment, see Burch et al. (2016).

The intermediate output of MRs and associated tearing mode instabilities is constituted by strings of "magnetic islands" or plasmoids, many of which then merge into a few giant ones. Meanwhile, on the *kinetic* side sharply sheared or even annihilating B-lines induce strong if confined E-lines; these repeatedly and efficiently accelerate electrons in situ to high values of $\gamma \sim 10^3$, particularly around the giant, coalescing plasmoids and in the intervening gaps. Next we focus on the key parameters governing these two related sides of the processes occurring in magnetized jets.

3.1. The Macroscopic Side

The relevant parameter for stability on large scales is provided by the *bulk* magnetization of the jet

$$\sigma_j = \frac{\bar{B}^2}{4\,\pi\, n_p\, m_p\, c^2\, \Gamma^2} \tag{1}$$

(see Kennel & Coroniti 1984). This depends on the average field that appears in the agnetic stress $\bar{B}^2/4\,\pi$, and on the kinetic stress $n\, m_p\, c^2\, \Gamma^2$ dominated by the jet protons (see Celotti & Ghisellini 2008).

The condition $\sigma_j \lesssim 1$ yields stability of a jet on large scales —for example, on the scales 10^{16}–10^{17} cm numerically investigated by Mignone et al. (2013). On the other hand, values $\sigma_j \gtrsim 1$ are found by the same authors to promote jet instabilities. Thus the magnetization σ_j constitutes the main

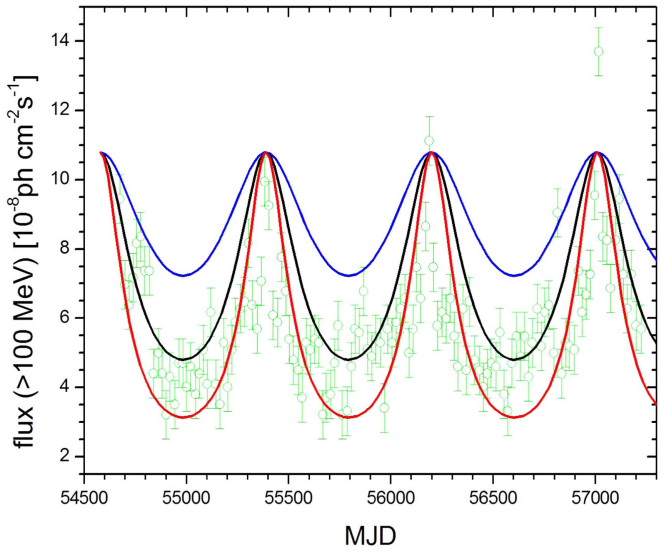

Figure 2. The gamma-ray light curve of PG 1553+113 (green data points and error bars from A15) is compared with the predictions from our model, in which the gamma-ray flux is proportional to the gravitational force after $f(t) \propto F(r)/F(r_{\max})$ (see Equation (4) in the Appendix) along the elliptical orbit at a distance r from the focus. We used the apparent period $P = 2.2$ year (see Section 4.2) and three values for the eccentricity: $\epsilon = 0.1$ (blue curve), $\epsilon = 0.2$ (black curve), and $\epsilon = 0.3$ (red curve). For $\epsilon = 0$, the orbit would be circular and the light curve just flat, apart from minor random fluctuations.

parameter governing the overall stability of a jet configuration on large scales.

Using values of $B \sim (0.1\text{–}1)$ G, $n \sim 10^{-1}$–10^{2} cm^{-3} related to the accretion rates on the primary SMBH, and values $\Gamma \sim 10$, as derived, for example, by Paggi et al. (2009), Tavani et al. (2015), and observed by Hovatta et al. (2009), we find $\sigma_j < 10^{-1}$ to hold in FSRQs, while $\sigma_j \lesssim 1$ prevails in BL Lacs. Thus the latter appear to sit on the brink of instability, and may be driven *unstable* by minor dynamical perturbations such as may be induced by a binary BH companion. On evaluating at $T/10$ (details are given in the Appendix), the period fraction with strong primary acceleration while revolving around the barycenter, it is seen that the jet cannot remain connected over scales $\ell > cT/10 \sim 10^{17}$ cm against dynamical perturbations that shake its base on an effective timescale of a few months. This also sets an upper limit to any spread along the axis of the sources of correlated emissions.

3.2. The Kinetic Side

At the opposite extreme constituted by the local *kinetic* level, acceleration of electrons to high energies is governed by repeated MR events. The acceleration process has been parametrized and numerically computed in terms of the electron *local* magnetization (see the review of Kagan et al. 2015),

$$\sigma_e = \frac{B^2}{4\,\pi\, n_e\, m_e\, c^2}, \tag{2}$$

which depends on the *local* magnetic field B and electron density $n_e = n_p$, given their mass m_e.

Many numerical calculations have been carried out in the range of σ_e values from tens to up to several hundreds (see Melzani et al. 2014; Sironi & Spitkovsky 2014). Remarkably, for increasing $\sigma_e > 10^2$ the resulting electron energy distributions approach flat power-laws $n(\gamma) \propto \gamma^{-1.5}$ up to or asymptotically exceeding $\gamma \sim 10^3$, limited by computing times (e.g., Melzani et al. 2014). We stress that for comparable local and average strengths of the magnetic field, the relation

$$\sigma_e = \frac{m_p}{m_e}\Gamma^2\,\sigma_j \sim 10^4\,\sigma_j \tag{3}$$

holds, so that the electron energies can grow to values $\gamma \sim 10^3$ and possibly beyond as soon as bulk instability conditions are established by values[5] of $\sigma_j > 1$. In other words, conditions conducive to bulk instability act as a *trigger* for strong particle accelerations to occur. Note, however, that the electron magnetization in Equation (2) affects the particle energy distribution function only in the presence of *topological* configurations of the local magnetic field that include sheared layers or close reversals conducive to tearing and reconnections in the jet's collisionless plasma.

Extensive and detailed computations have recently been presented by Yuan et al. (2016), concerning the link between macroscopic field configurations with higher magnetization and kinetic conditions conducive to acceleration. We conclude that a slow *time* shift of macroscopic conditions toward increased σ_j and sheared B topology can *end up* into triggering and enhancing local accelerations governed by high values of σ_e.

3.3. The Binary Drive

Thus current knowledge backs our expectation that in BL Lac jets—by themselves in near-critical conditions—even modest perturbations that increase B can easily drive the structure beyond the threshold of macroscopic instabilities. Soon after, the conditions will progress toward strong kinetic instabilities if the macroscopic modes induce local torsion and shear of B. The ensuing scale for field shearing will be close to the longitudinal mode wavelengths experienced by the jet, which are of order of 10^{16}–10^{17} cm as numerically computed, for example, by Mignone et al. (2013; see also Striani et al. 2016).

In the case of a binary SMBH system, we envision as a *driving* agent the dynamical perturbations of the magnetic jet configuration by the companion orbiting around the accretion disk, from which the main jet is launched. When the perturbations occur, the field $\boldsymbol{B}$ not only is locally *compressed* to larger strength $B + \delta B \simeq$ a few times B, but also is locally *sheared* so that regions of sharply different magnetic field lines are drawn together.

In a nutshell, binary perturbations *drive* macroscopic jet instabilities that offer many suitable locations for MR to occur and *trigger* effective electron acceleration; the ensuing emissions are detailed next.

4. Emissions and Their Interpretations

The basic feature to be expected from the binary drive of jet instabilities as discussed in Section 3 concerns a recurring, nonlinear spike–trough pattern in the light curves, reflecting the stroke–relaxation nature of the dynamical drive along a Keplerian elliptical orbit.

[5] Note that Equation (3) as it stands applies for values of $\gamma \lesssim m_p/m_e$. For larger values, the electron contribution to the total kinetic energy should not be neglected; σ_j is correspondingly decreased, and so is the effective σ_e. This feature may imply self-regulation to limiting energies $\gamma \sim 10^4$.

Table 1
Parameters for Modeling the Spectral States of PG 1553+113

State	*Comp.*	Γ	$\boldsymbol{B}$ (G)	$\boldsymbol{R}$ (cm)	$\boldsymbol{K}$ (cm^{-3})	γ_b	$\gamma_{\rm min}$	α_1	α_2
Low	gray	15	0.25	4.0×10^{16}	0.6	9×10^3	4×10^3	2	3.9
Enhanced Soft	red	15	0.29	4.0×10^{16}	0.6	9×10^3	3×10^3	2	3.9
Enhanced Hard	blue dashed	15	0.29	3.5×10^{16}	0.1	3×10^4	5×10^3	2	4.3

Note. The table summarizes the parameters used in our SSC spectral modeling of PG 1553+113 (see Figure 3). The table provides values for the bulk Lorentz factor Γ, the average magnetic field B inducing synchrotron emission, the source size R, the electron energy distribution $n(\gamma) = K\ \gamma_b^{-1}\ (\gamma/\gamma_b)^{-\alpha}$ with normalization K, upper break at γ_b and lower bound $\gamma_{\rm min}$, and power-law indices α_1 below and α_2 above the break. The associated cooling times for S and for IC (see Rybicki & Lightman 1979) read $t_c \simeq 2\,R/c \simeq 30$ day.

4.1. Light Curves

To be specific, we will refer to the BL Lac object PG 1553 +113 as an interesting candidate for recurrent nonlinear gamma-ray emission, as observed and discussed by A15. The source features in its *continuously* monitored gamma-ray emission high amplitude modulations that recur with an apparent period $P \simeq 2.2$ year; at the source redshift $z \simeq 0.5$ (see Danforth et al. 2010), this corresponds to an intrinsic value $T \simeq 1.5$ year. Three full (in fact, 3.5) consecutive periods are continuously covered by the existing gamma-ray data of PG 1553+113 presented in A15; these data extend the dynamic range (number of cycles and modulation features) of previous blazar periodicity analyses such as those of Vaughan et al. (2016). From the A15 analysis of PG 1553+113, the next gamma-ray peak is expected in early 2017.

In the Appendix we derive in detail a simple model for the gamma-ray light curve based on the gravitational modulation in a binary system, as impressed by the companion on the primary BH and its associated jet. Our result is presented here in Figure 2, along with the 7 year data concerning PG 1553 +113 from A15. It is seen that our model yields a *nonlinear* pattern of the light curve with prominent peaks and wide troughs, which for an eccentricity $\epsilon \simeq 0.2$ is quantitatively very close to the overlaid data points.

4.2. Spectral Distributions

The basic spectral change expected from compressed and sheared magnetic fields in the jet is twofold. Initially, we expect an increased overall SSC emissivity, led by the optical S emission and followed after some weeks by IC radiation at GeV energies. Such a direct correlation is well compatible with the data, as discussed by A15, but is also expected to be appreciably smeared out along the jet axis by outflow and long cooling times for both component sources (see Table 1 and its caption).

In detail, the implied enhancements of S optical radiation and of its IC counterpart at GeV energies are shown by the spectra marked in red in Figure 3 with overlaid data. Such flux variations in both the R-band and the GeV component range by a factor around 3 from minima to maxima. In conclusion, the emissions in the optical, the soft X, and the GeV bands appear to generally correlate along the spectra in shape and timing in the way described by the canonical SSC radiation model.

On the other hand, the behavior at keV energies of PG 1553+113 appears to stray outside the previously described framework, and has been reported as "enigmatic" (see, e.g., Raiteri et al. 2015). For one, the increases during episodes of optical rise differ in softer X-ray ranges: they rise from a factor of 3 in the range 0.3–2 keV, but are up to factors

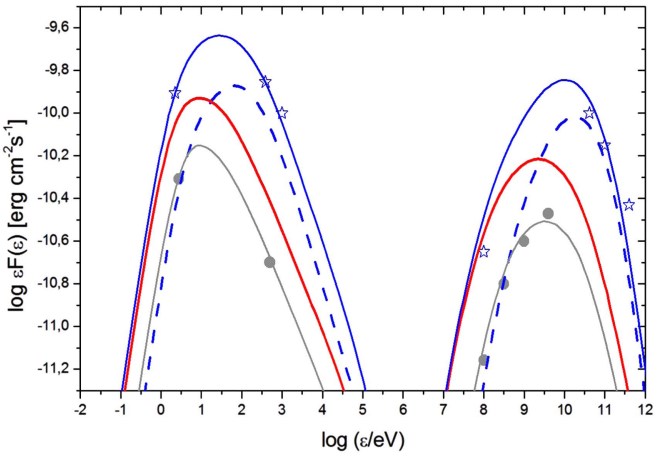

Figure 3. Spectral energy distribution (SED) of the emissions by electrons accelerated in the jet of the BL Lac PG 1553+113. Spectral data are from Ackermann et al. (2015) and Aleksic et al. (2015). The gray line shows the spectral state during normal conditions. The blue, dashed curve represents the *harder* increased synchrotron and IC components resulting from the extra electron acceleration discussed in Section 4.3. The total emission in the *enhanced* state is represented by the blue solid curve. EBL de-absorption in the TeV data after Aleksic et al. (2012).

5–10 in the 2–10 keV range, as reported by Aleksic et al. (2015), for the episode around MJD 56,000. In addition, other BL Lacs such as Mkn 421 appear to share with PG 1553 +113 such keV features as missing correlation with neighboring X-rays, and positive correlations with TeV emissions (Balokovic et al. 2016).

4.3. An Additional Spectral Component in X-Rays

To interpret such a behavior, we recall the contents of Section 3. In particular, in Section 3.1 we noted that a BL Lac jet is normally metastable, so that a limited increase of B can drive it first toward macroscopic, and then into kinetic instability conditions.

In the initial stage, the near-critical bulk magnetization $\sigma_j \lesssim 1$ is increased by a factor of a few, as deduced from the optical light curves enhanced during their 100 day rise. This implies a drift from marginal values of σ_j into the fully critical range for macroscopic instabilities. If these produce twisted and inverted $\boldsymbol{B}$ lines, a second stage arises, driven by increasing local magnetizations $\sigma_e \propto \sigma_j$ after Equation (3). These enhance MRs and cause extensive particle acceleration. Based on current numerical simulations that are exploring different regimes of ion-electron plasmas (see Melzani et al. 2014; Kagan et al. 2015), we derive that the maximal electron energies can approach values $\gamma_p \sim 10^4$ for values of σ_e

exceeding 10^2. Such enhanced accelerations will *add* a stronger and harder spectral component in the X-ray range around and above 1 keV, as indeed detected in at least two episodes within the currently available data concerning PG 1553+113 (A15). The X-ray flux increase amounts to factors of 5–10 (i.e., substantially *larger* than the related rise of optical and GeV emissions). Clearly, here one-zone, single population modeling of the X-ray emission together with the optical and GeV emissions would not be adequate. Our picture, on the other hand, implies additional particle acceleration triggered in nearby zones with increasing values of σ_e. The corresponding SEDs for one such episode are presented in Figure 3.

5. Discussion and Conclusions

We have argued in Section 2 that dynamic events in blazar jets—and specifically in BL Lac objects—originate from an underlying binary system of two supermassive black holes with total mass $M \sim 10^8\, M_\odot$. Binary dynamics constitutes, as we stated in Section 2 and explained in Section 3, the prime mover for a chain of events in the jet: it recurrently drives bulk plasma instabilities in the metastable magnetized jet launched by the primary; in turn, these trigger local tearing instabilities and in situ electron acceleration to high energies corresponding to, and at times exceeding, $\gamma \sim 10^3$.

Such local instabilities and accelerations are known to arise in narrow layers of a collisionless plasma, where reconnections occur among adjacent B-lines that are strongly sheared or even reversed, as we detailed in Sections 3.1 and 3.2. Such processes are bound to be triggered during dynamic episodes of large-scale squeezing and shearing of a magnetized jet. A conducive context for such episodes to occur is provided by binary SMBH dynamics (as discussed in Section 3.3), which also provides the simplest interpretation for the recurrent, nonlinear pattern of peaks and trough in the light curves of the BL Lac source PG 1553+113, as discussed in Section 4.1.

We have analyzed in Section 4.2 the different spectral states that arise in this source and exhibit repetition. They start with a recurrent increase of the optical synchrotron and of the IC GeV radiations produced by the same population of energetic electrons. We have stressed in Section 4.3 the additional spectral component that has been observed in the keV range as the optical light curve approaches a peak. We traced it back to spreading accelerations triggered by additional reconnections stimulated by binary dynamics. We expect this component to correlate with TeV enhancement, as occurs in other BL Lacs.

So we conclude that, at times, two spectral states overlap in the emissions from PG 1553+113. One is well represented as a quasi-periodic emission that envisages the optical–soft X-ray components and the GeV photons as linked components of the same SSC radiation process; the latter therefore should correlate with the former, after a lag of some weeks. The other, more energetically demanding state requires additional and higher electron accelerations that produce a harder X-ray peak, as a component (see Section 4.3) observed in two out of three monitored instances. This we expect to correlate with TeV enhancements, not necessarily with the optical–GeV radiations.

Next we summarize our overall conclusions, and specifically two points. First, we have described how a BL Lac jet, normally sitting on the brink of instability, can undergo recurrent stresses from the binary dynamics sufficient to stimulate cyclic emissions. In fact, increasing bulk magnetization leads to large-scale instabilities that cascade down to small scale MRs and ultimately percolate to the kinetic level; there they accelerate the electrons that emit from the optical to the gamma-ray band, and sometimes beyond.

Second, the binary Keplerian motion drives strokes and allows relaxations corresponding to orbital arcs both close to and far away from the periastron, respectively. So it imprints a specific nonlinear pattern of sharp peaks and wide troughs in the light curves at different frequencies; these are particularly sharp in gamma-rays that have been continuously monitored from space. Such a pattern can provide diagnostics for orbital parameters, in particular for the orbital eccentricity ϵ as detailed in the Appendix and used in Figure 2 to derive a value $\varepsilon \simeq 0.2$ for PG 1553+113.

Regarding predictions and prospects, in the framework of the next gamma-ray peak expected for PG 1553 in early 2017 by A15, we stress the following points. (1) The new peak should appear in reasonable phase agreement (within the time binning) with the previous three occurrences. (2) Thus the optical emission should be monitored as continuously as possible across the peak phase range, with the help of strategically coordinated telescopes. The optical emission may be quite structured, as shown by Figures 1 and 2 of A15; in our picture we expect the main optical increase to begin several days to some weeks before the smoother and better sampled gamma-ray peak, which can sound a last call (as it were) for aimed X-ray observations. (3) In fact, the X-ray extra component in the keV range is expected to be triggered by expanding reconnections that occur just at or on the approach to the periastron. Current data have the peak of additional X-ray emission corresponding in one case to the gamma-ray peak near MJD 57000 (to within the time binning), and in another case, preceding the gamma-ray peak by ∼100 days. Our model contemplates enhanced keV emission somewhere between the rise of the optical and of the gamma-ray light curves, on account of the spread along the jet of the S and the IC main sources implied by their long cooling times (see Section 4.3, and Table 1). It is interesting to recall that a similar radiative behavior to PG 1553+113 is shared by other BL Lacs, in particular by Mrk 421, with its long, puzzling X-ray outbursts correlated with TeV activity but not with optical and GeV emissions (see Raiteri et al. 2015; Balokovic et al. 2015). Some of these sources (listed, e.g., by Sandrinelli et al. 2014) have been proposed also as candidates for recurring behavior in the optical and gamma-ray bands.

We note that the current apparent dominance of claimed or suspected BL Lacs periodicities over FSRQs may just reflect selection favoring BL Lacs on account of their relatively small distances and lack of disturbing O-UV background from broad optical lines and BBB.

On the other hand, as a consequence of hierarchical galaxy formation, the BL Lacs as *long-lived* AGNs (Cavaliere & D'Elia 2002; also Böttcher & Dermer 2002) must have witnessed quite a number of merging events involving their host galactic nuclei. Thus, expanding on the pioneering suggestion by Begelman et al. (1980), such nuclei would be more massive, and more likely to have accrued SMBHs to form a dominant binary pair. Such an environmental condition adds to the intrinsic metastability of BL Lac jets discussed in Section 3 that makes them susceptible even to minor dynamic disturbances. In the perspective of 10^6 years, the systems'

lifetimes and effective statistics will be limited by gravitational and electromagnetic losses.

Finally, we consider the A15 prediction concerning a next maximum of PG 1553+113 in early 2017, with a spread of some 20–40 days due to time binning; this would mark an obvious plus for the periodic view. On the quantitative side, extending the sequence of fully observed cycles from 3 to 4 would considerably strengthen the confidence level 0.99 recalled in Section 4. Thus by 2017 one had better be prepared with astrophysical analysis of the currently known periods as undertaken here, and with coordinated observations of keV–TeV emissions. We add that evidence of any secondary jet would provide a telltale signature of binarity that deserves a close investigation, despite a number of difficulties: the expected weak power ratio $\propto M_2/M_1 \sim 10^{-1}$ even in the favorable case of both jets fed by accretion at a common fraction of their Eddington rates; the uncertainty about the jet relative angle; and the range in the time phase caused by precessional shifts.

These tasks are demanding, but the reward of any strong evidence for binarity would be worth keen observational efforts. It is generally agreed that understanding even a single SMBH binary would open a new window on the vexing issue of co-evolution of galaxies and their central BHs (see Lapi et al. 2014; Volonteri et al. 2015). In addition, a few confirmed SMBH binaries with assessed orbital parameters such as proposed here may be of considerable value for planning searches of giant, slow bursts of gravitational waves with space interferometers such as eLISA (see eLISA Consortium 2013). In fact, the path from host galaxy mergers to a sub-pc binary doomed to eventually coalesce is complex (see Colpi 2015) and currently still fraught with a number of uncertain steps ("stalling" in particular) that not even massive numerical computations or simulations have been able to fix to now.

We are indebted to Bruno Coppi for enlightening discussions on magnetic field reconnecting structures in collisionless plasmas. We thank our referee for recommending a generally conservative attitude toward the quasi-periodicity of PG 1553+113, and for pressing us to specify the role of light curve profiles, as we did in the revised manuscript. Work partially supported by the ASI grant no. I/028/12/2.

Appendix
Deriving the Light Curves and the Corresponding Orbital Eccentricity

In Section 3 we consider a gravitationally bound binary system with separation of several milli-pc. Drawing on time-honored dynamical relations holding for Keplerian, elliptical orbits of the secondary (see, e.g., Landau & Lifshitz 1976, and their Figure 11) compared with the light curves observed by A15 (cf. their Figures 1 and 2), we detail how we deduce our expected light curve and the corresponding orbital eccentricity, ε.

We will follow two methods. For simplicity, in both we neglect the primary motion around the system's center of mass, and in particular the size of its obit that scales as $M_2/M_1 \lesssim 10^{-1}$. We base this on the gravitational stress from the secondary being proportional to the force between the two BHs, with enhanced emission also proportional to it.

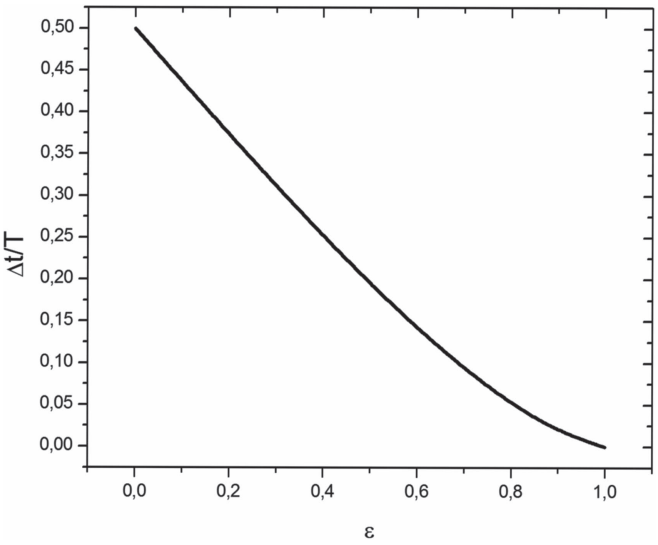

Figure 4. The ratio $\Delta t/P$ plotted as a function of the eccentricity for a Keplerian elliptical orbit. This quantity marks the strongly active fraction of the orbital period, which we take to be the interval between the intersections of the "latus rectum," each side of the periastron.

(1) The ratio of the force at periastron to that at the opposite vertex reads

$$F_{\max}/F_{\min} = (1+\varepsilon)^2/(1-\varepsilon)^2. \quad (4)$$

In our approach, this also yields the ratio of gamma-ray fluxes at maxima and minima.

From the gamma-ray light curve in A15 (their Figure 1), we read out the observed value $\simeq$3 for the flux ratio between peaks and troughs. After Equation (4) this corresponds to an orbital eccentricity $\varepsilon \simeq 0.25$.

In addition, in Figure 4 we plot the full dependence $f(t) \propto F[r(t)]$ of flux that we expect along the orbit at a distance $r(t)$ from the focus, parameterized with three eccentricity values: $\epsilon = 0.1, 0.2, 0.3$. The data are overplotted, and agreement is found for $\epsilon = 0.2$.

(2) A second approach considers the time fraction along the orbit most affected by such an effect. For an estimate, we concentrate on the points on the elliptical orbit marking the intersections with the so-called *latus rectum* p (i.e., the orbital distance corresponding to the "true anomaly" angle $\phi = \pi/2$, with $\phi = 0$ at periastron). The time Δt spent on the orbital arc circling the focus from p through the periastron out to the opposite phase is given by

$$\frac{\Delta t}{P} = \frac{\arccos(\varepsilon) - \varepsilon\sqrt{1-\varepsilon^2}}{\pi}. \quad (5)$$

Figure 4 shows the ratio $\Delta t/P$ as a function of orbital eccentricities. From the observations recalled previously we see that the strongly enhanced emission lasts for $\sim$280 days, corresponding to a fraction $\Delta t/P \simeq 0.35$. Interpreting this feature as caused by the gravitational perturbation of a secondary BH in an elliptical orbit, we deduce from Figure 4 a value of the eccentricity $\varepsilon \simeq 0.23$.

Thus we conclude that on interpreting the repetitive pattern of enhanced high-energy emissions from PG 1553+113 in terms of stresses induced by binary dynamics, both the previously listed approaches lead us to evaluate for the orbital eccentricity a value close to $\varepsilon = 0.2$.

Note that for a circular orbit the expected light curve is just flat; in fact, from Equation (4) one obtains $F_{\max}/F_{\min} = 1$. Concerning Figure 2 in the main text, we stress that the dynamically *stimulated* (as it were) emission maxima largely exceed the *spontaneous* random fluctuations best noticed in the troughs.

References

Abbott, B. P., Abbott, R., Abbott, T. D., et al. 2016a, PhRvL, 116, 061102
Abbott, B. P., Abbott, R., Abbott, T. D., et al. 2016b, PhRvL, 116, 241103
Ackermann, M., Ajello, M., Albert, A., et al. 2015, ApJL, 813, L41
Aleksic, J., Alvarez, E. A., Antonelli, L. A., et al. 2012, ApJ, 748, 46
Aleksic, J., Ansoldi, S., Antonelli, L. A., et al. 2015, MNRAS, 450, 4399
Balokovic, M., Matt, G., Harrison, F. A., et al. 2015, ApJ, 800, 62
Balokovic, M., Paneque, D., Madejski, G., et al. 2016, ApJ, 819, 156
Baumgarte, T. W., & Shapiro, S. L. 2011, PhT, 64, 32
Begelman, M., Blandford, R. D., & Rees, M. J. 1980, Natur, 207, 307
Böttcher, M., & Dermer, C. D. 2002, ApJ, 564, 86
Burch, J. L., Torbert, R. B., Phan, T. D., et al. 2016, Sci, 352, 1189
Cavaliere, A., & D'Elia, V. 2002, ApJ, 571, 226
Celotti, A, & Ghisellini, G. 2008, MNRAS, 385, 283
Colpi, M. 2014, SSRv, 183, 189
Colpi, M. 2015, Available online at http://www.cosmos.esa.int/web/conferences-archive/athena-2015
Coppi, B. 2016, PlPhR, 42, 383
Danforth, C. W., Keeney, B. A., Stocke, J. T., Shull, J. M., & Yao, Y. 2010, ApJ, 720, 976
eLISA Consortium 2013, The Gravitational Universe, arXiv:1305.5720v1
Ghisellini, G. 2016, arXiv:1609.08606
Hovatta, T., Valtaoja, E., Tornikoski, M., & Lahteenmäki, A. 2009, A&A, 494, 527
Kagan, D., Sironi, L., Cerutti, B., & Giannios, D. 2015, SSRv, 191, 545
Kelly, B. C., Bechtold, J., & Siemiginowska, A. 2009, ApJ, 698, 895
Kennel, C. F., & Coroniti, F. V. 1984, ApJ, 283, 694
Landau, L., & Lifshitz, E. M. 1976, Mechanics (Oxford: Pergamon)
Lapi, A., Raimundo, S., Aversa, R., et al. 2014, ApJ, 782, 69
Maraschi, L., Ghisellini, G., & Celotti, A. 1992, ApJ, 397, L5
Melzani, M., Walder, R., Folini, D., et al. 2014, A&A, 570A, 111
Mignone, A., Striani, E., Tavani, M., & Ferrari, A. 2013, MNRAS, 436, 1102
Nixon, C., & King, A. 2015, arXiv:1505.07827
Paggi, A., Cavaliere, A., Vittorini, V., & Tavani, M. 2009, A&A, 508, L31
Palenzuela, C., Garrett, T., Lehner, L., & Liebling, S. L. 2010, PhRvD, 82, 404
Peterson, B. M. 1997, An Introduction to Active Galactic Nuclei (Cambridge: Cambridge Univ. Press)
Raiteri, C. M., Stamerra, A., Villata, M., et al. 2015, MNRAS, 454, 353
Rybicki, G. H., & Lightman, A. P. 1979, Radiative Processes in Astrophysics (New York: Wiley)
Sandrinelli, A., Covino, S., & Treves, A. 2014, A&A, 562, 79
Sironi, L., & Spitkovsky, A. 2014, ApJL, 783, 21
Striani, E., Mignone, A., Vaidya, B., Bodo, G., & Ferrari, A. 2016, MNRAS, 462, 2970
Tavani, M., Vittorini, V., & Cavaliere, A. 2015, ApJ, 814, 51
Urry, C. M., & Padovani, P. 1995, PASP, 107, 803
Vaughan, S., Uttley, P., Markowitz, A. G., et al. 2016, MNRAS, 461, 3145
Volonteri, M., Bogdanovic, T., Dotti, M., & Colpi, M. 2015, Proc. of the IAU XXIX General Assembly, Astronomy in Focus, Vol. 29B, 285
Yuan, Y., Nalewaiko, K., Zrake, J., East, W. E., & Blandford, R. 2016, ApJ, 828, 92